ACS OMEGA

http://pubs.acs.org/journal/acsodf

Article

Synergistic Flame Retardancy of Microcapsules Based on Ammonium Polyphosphate and Aluminum Hydroxide for Lithium-Ion Batteries

Teng-Kun Ma, Yu-Man Yang, Jia-Jia Jiang,* Meng Yang, and Jun-Cheng Jiang

Cite This: *ACS Omega* 2021, 6, 21227−21234

Read Online

ACCESS | Metrics & More | Article Recommendations

ABSTRACT: Flame retardants have important theoretical research and applied value for lithium-ion battery safety. Microcapsule flame retardants based on ammonium polyphosphate (APP) and aluminum hydroxide (ATH) were synthesized for application in lithium-ion batteries. First, the ATH−APP was prepared by coating a layer of ATH on the surface of the core APP. Then, the ATH−APP was encapsulated by poly(urea-formaldehyde) (PUF) to obtain en-ATH−APP. The structure and flame-retardant property of en-ATH−APP, the influence of en-ATH−APP on the thermal stability of the electrode, and the electrochemical performance of the battery were studied. The results of Fourier transform infrared and scanning electron microscope experiments indicated that APP was coated with ATH and PUF in turn. The results of differential scanning calorimetry and the fire extinguishing test for electrodes manifested that en-ATH−APP had better flame-retardant property than APP because of the synergistic effect between APP and ATH. Moreover, the flame-retardant efficiency of en-ATH−APP was comparable to that of ATH−APP, indicating that the presence of PUF had almost no effect on the flame-retardant property. The results of electrochemical experiments indicated that en-ATH−APP had the best electrochemical compatibility for the battery compared with APP and ATH−APP. The research lights the way to improve inherent safety of lithium-ion batteries by adding en-ATH−APP to the cathode.

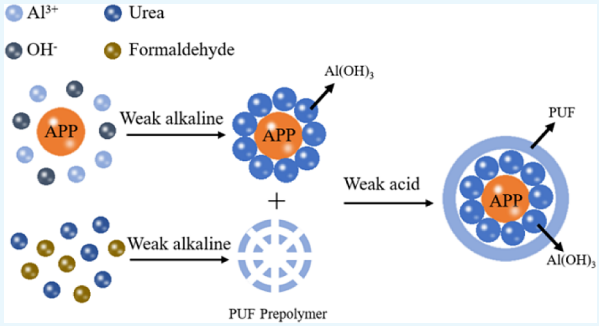

1. INTRODUCTION

Lithium-ion batteries are widely used in electric vehicles, portable devices, grid energy storage, and so forth, especially during the past decades because of their high specific energy density and charging rate. However, the safety of lithium-ion batteries is the stumbling block that restricts their large-scale application. The safety problem is mainly manifested in the fire caused by the thermal runaway because of overcharging, short circuits, and impacts,[1−5] which is a great challenge for the development of lithium-ion batteries. Methods to improve the safety of lithium-ion batteries include the modification of electrolyte,[6−8] surface treatment of separators,[9,10] modification of the cathode,[11] development of battery management systems,[12] and application of flame retardants. The application of flame retardants is one of the most simple and effective methods, which has been widely studied in recent years.

Alkyl phosphates, such as trimethyl phosphate, triethyl phosphate, and tributyl phosphate,[13−15] are early flame retardants for lithium-ion batteries, which have good flame-retardant effect but reduce the ionic conductivity of the electrolyte and shorten the cycle life of the batteries because of their high viscosity and poor compatibility with electrode materials (especially carbon-based anodes). To improve the electrochemical compatibility of phosphate esters, aromatic (phenyl) groups are used to partially replace alkyl groups. One of the most representatives is triphenyl phosphate (TPP).[16] However, the influence of flame retardants on the electrochemical property is inevitable when it is directly added to the battery. A novel method is proposed to improve the electrochemical property by microencapsulated flame retardants. Chen and Li[17] microencapsulated aluminum hydroxide (ATH), boehmite (AlOOH), and TPP by poly(urea-formaldehyde) (PUF). The results of electrochemical experiments manifested that the compatibility of flame retardants with the electrode material was improved when flame retardants were coated with PUF. Huang et al.[18] encapsulated TPP and 9,10-dihydro-9-oxa-10-phosphaphenanthrene 10-oxide (DOPO) individually by PUF. The electrochemical measurements showed that cathodes with en-TPP and en-DOPO exhibited

Received: February 2, 2021
Accepted: May 26, 2021
Published: August 11, 2021

https://doi.org/10.1021/acsomega.1c00598
ACS Omega 2021, 6, 21227−21234

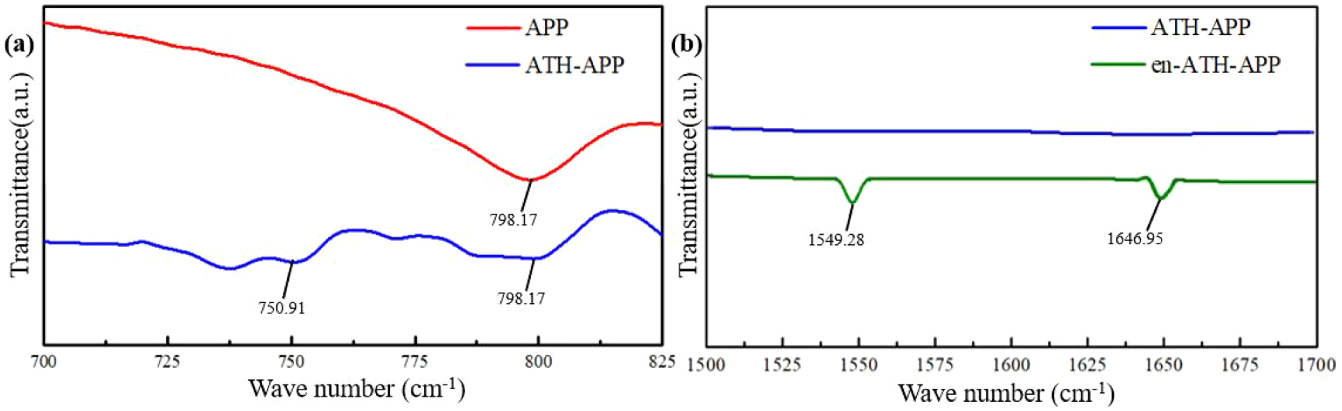

Figure 1. FTIR spectra of (a) APP and ATH−APP and (b) ATH−APP and en-ATH−APP.

a much lower impedance and higher capacities compared with those containing TPP and DOPO. Baginska et al.[19] encapsulated tris(2-chloroethyl phosphate) by PUF. The microcapsules were electrochemically stable in lithium-ion battery electrolytes and thermally stable at 200 °C.

Ammonium polyphosphate (APP) is an efficient intumescent flame retardant, which achieves the flame-retardant effect in solid phases and gas phases.[20] ATH is an inorganic flame retardant, which exhibits high endothermic reaction when it decomposes.[21] APP and ATH have been widely used in polymer materials (such as polypropylene[22] to improve the flame-retardant property. It is found that ATH and APP have better flame retardancy when used together because of the synergism mechanism.[23] In this work, a synergistic flame-retardant microcapsule based on APP and ATH was prepared and added to the electrode of lithium-ion batteries. ATH encapsulated APP by the method of precipitation (denoted as ATH−APP) to achieve the synergy of ATH and APP. PUF was used to microencapsulate ATH−APP to reduce the negative effect of ATH−APP on the electrochemical property of the battery. The effect of microcapsule flame retardants on the safety of the electrode was tested by differential scanning calorimetry (DSC) and the fire extinguishing test. The electrochemical properties of the battery were tested by the battery discharge capacity and impedance. The experimental results manifested that the prepared microcapsule flame retardants could improve the safety of lithium-ion batteries in the initial stage of thermal runaway while ensuring their electrochemical properties.

2. RESULTS AND DISCUSSION

2.1. Encapsulation of Flame Retardants. The phosphorus flame-retardant APP was encapsulated by ATH and PUF in turn. The Fourier transform infrared (FTIR) spectra of APP, ATH—APP, and en-ATH—APP are compared in Figure 1. It is obvious that the new infrared absorption peak (spectrum ATH—APP) appeared at 750 cm^{-1}, as shown in Figure 1a, which corresponds to the asymmetric vibration of Al—O.[24,25] The spectra of ATH—APP and en-ATH—APP are shown in Figure 1b. The new absorptions peaks (spectrum en-ATH—APP) at 1647 and 1549 cm^{-1} correspond to the stretching vibrations of —C═O and —C—N— induced by PUF, respectively.[26]

The morphologies of APP, ATH−APP, and en-ATH−APP are shown in Figure 2. As shown in Figure 2b, the surface of the APP is smooth. The ATH−APP in Figure 2d shows an

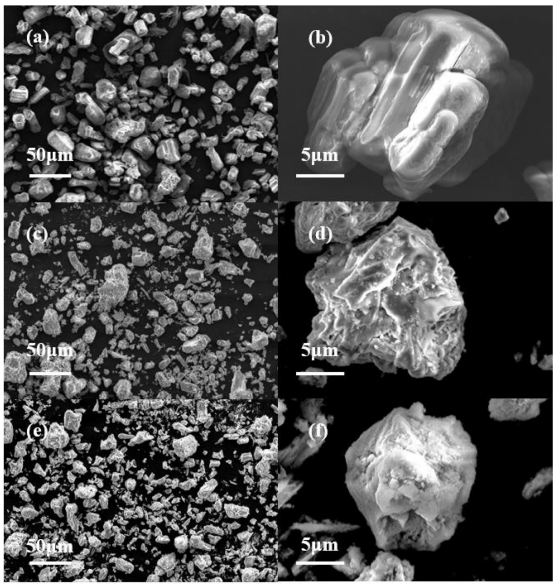

Figure 2. SEM images of (a,b) APP, (c,d) ATH−APP, and (e,f) en-ATH−APP.

uneven surface, which is due to the presence of ATH. The scanning electron microscopy (SEM) image of en-ATH−APP is shown in Figure 2f. The uneven surface of ATH−APP appears as a layer of flocculent material, which indicates the existence of PUF. The results of SEM and FTIR prove that the APP is microencapsulated after a series of chemical reactions.

2.2. Thermal Stability Test of the Electrode with Microcapsule Flame Retardants. The heat flow curves of $LiFePO_4$−electrolyte mixture with 0% state of charge (SOC) are shown in Figure 3. The mixture has a sharp exothermic peak at 121−163 °C, and the total released heat of the mixture is 102 J g^{-1}. After adding flame retardants, the heat flow curves shift to the right, indicating that the initial exothermic temperature of the mixture increases. The released heat is reduced from 102 to 91, 66, and 75 J g^{-1}, respectively, when 5 wt % APP, ATH−APP, and en-ATH−APP are added to the cathode material, as shown in Figure 3a. The released heat is further reduced to 81, 57, and 63 J g^{-1}, respectively, when the flame-retardant content increases to 10 wt %, as shown in Figure 3b. The addition of microcapsule flame retardants not only increases the exothermic temperature of the mixture but also reduces the released heat of the mixture.

https://doi.org/10.1021/acsomega.1c00598
ACS Omega 2021, 6, 21227−21234

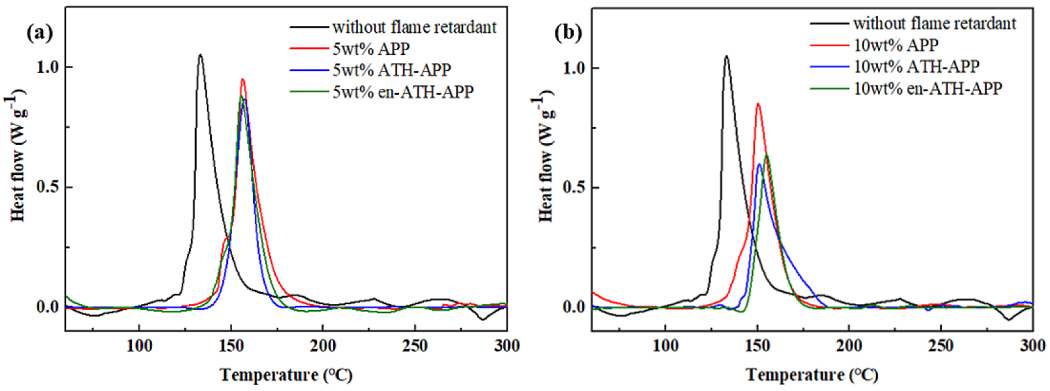

Figure 3. Heat flow curves of $LiFePO_4$−electrolyte mixture with 0% SOC.

The SOC is one of the important factors affecting the thermal stability of the cathode; hence, the $LiFePO_4$−electrolyte mixture with 100% SOC has also been tested by DSC, and the results are shown in Figure 4. Compared with

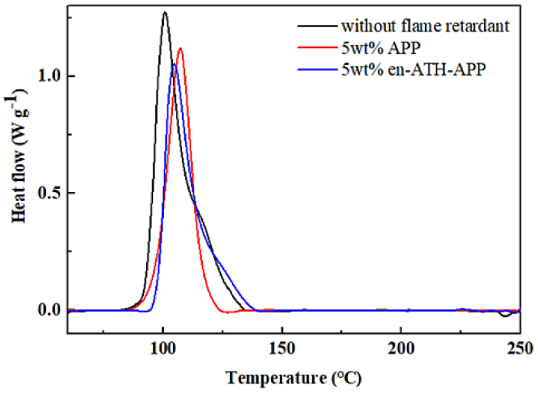

Figure 4. Heat flow curves of $LiFePO_4$−electrolyte mixture with 100% SOC.

0% SOC, the initial exothermic temperature of the mixture without the flame retardant decreased to 87 °C, and the total exothermic heat rises to 121 J g^{-1}. The released heat is reduced to 97 and 86 J g^{-1}, respectively, when the cathode contains 5 wt % APP and 5 wt % en-ATH−APP. In addition, the initial exothermic temperature shows a slight increase. Because of the synergistic effect of APP and ATH, en-ATH−APP has a better flame retardant effect than APP.

The effect of en-ATH−APP on the thermal stability of graphite anodes charged to 100% SOC has been further studied, and the DSC experimental results of graphite are shown in Figure 5. It can be seen that the heat flow curve of graphite without en-ATH−APP has a sharp exothermic peak at 136−178 °C and a weak exothermic peak at 222−278 °C, and the released heat is 212.26 and 40.3 J g^{-1}, respectively. Because of the synergistic flame retardant effect of APP and ATH, the released heat of the first exothermic peak is reduced to 181.3 J g^{-1} and the exothermic peak at 222−278 °C disappears when the graphite anode contains 5 wt % en-ATH−APP.

The addition of the microcapsule flame retardants reduces the released heat of the mixture, which can be explained by the decomposition of flame retardants. The main decomposition mechanism of APP is shown in Figure 6. The $-NH_4$ groups on APP decompose to produce ammonia (NH_3), which dilutes the oxygen concentration and achieves the purpose of

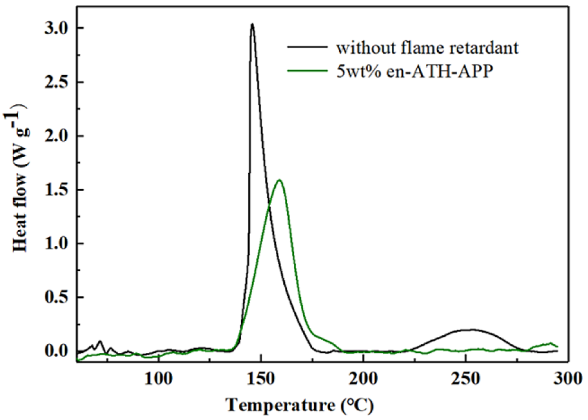

Figure 5. Heat flow curves of graphite anodes with 100% SOC.

suppressing combustion. Moreover, the polyphosphoric acid ($H_xP_yO_z$) produced by the decomposition of APP can cause dehydration and carbonization of the burning material, and the formed carbon layer inhibits the reaction between the cathode material and the electrolyte.

ATH−APP on the cathode material has better flame-retardant property because of the synergistic flame retardancy of ATH and APP. The synergistic flame-retardant effect between ATH and APP is shown in Figure 7.[27] ATH and APP react with each other, and the reaction can absorb a lot of heat. The reaction between the $-NH_4$ group in APP and the OH^- ion in ATH generates NH_3 and H_2O, which exert a flame-retardant effect in the gas phase. In addition, the solid product is $AlPO_4$, which plays a flame-retardant role in the solid phase by covering the surface of the cathode material.

2.3. Flame-Retardant Property Test of $LiFePO_4$−Electrolyte Mixture with Microcapsule Flame Retardants. The cathode material with flame retardants and the electrolyte were mixed at a mass ratio of 3:1, and then, the mixture was placed in a glass dish and ignited in the atmosphere to evaluate the flame-retardant efficiency of flame retardants. The combustion images of mixtures with different flame retardants are shown in Figure 8. It can be seen that the burning time of the mixture with en-ATH−APP is shorter than that of the mixture without flame retardants. Moreover, the higher the content of en-ATH−APP, the shorter the combustion time of the mixture.

The self-extinguishing time (SET) is the time taken by a unit mass of a material from the beginning of combustion to extinction. The SET of the mixture with 5 and 10 wt % flame

https://doi.org/10.1021/acsomega.1c00598
ACS Omega 2021, 6, 21227−21234

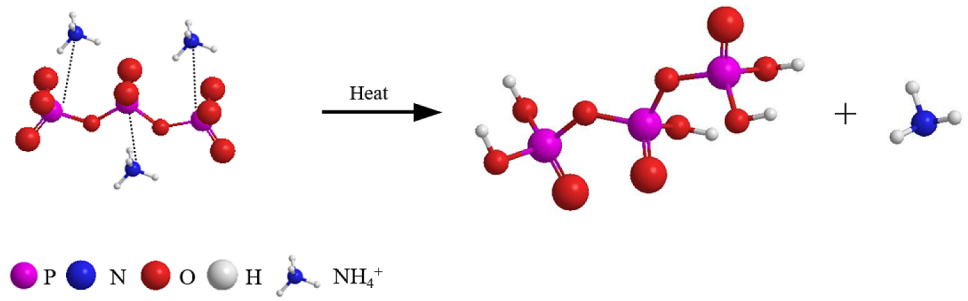

Figure 6. Decomposition mechanisms of APP.

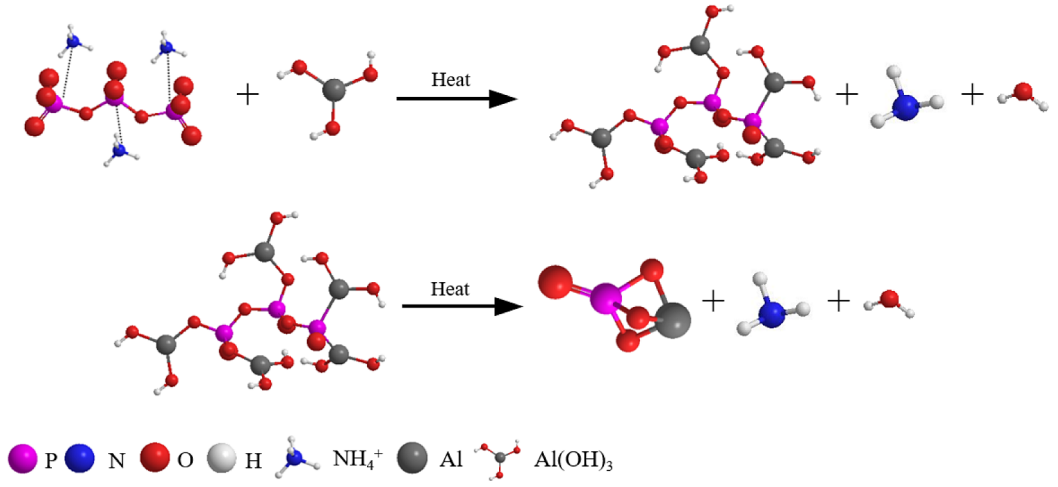

Figure 7. Reaction process between ATH and APP.

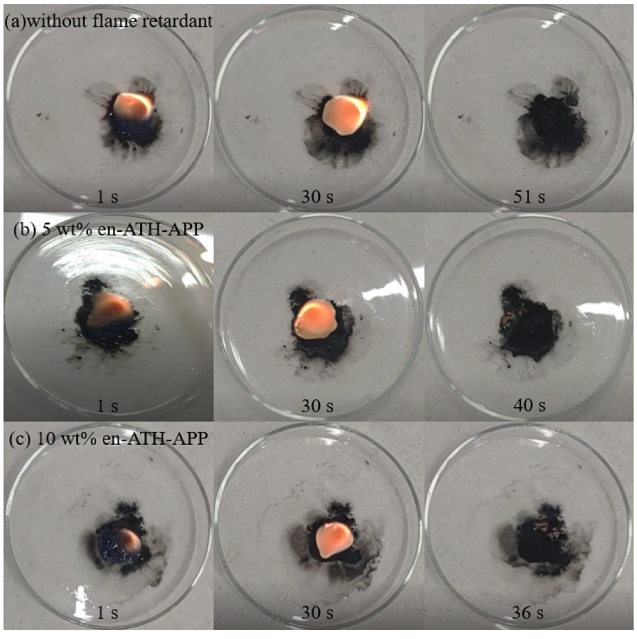

Figure 8. Combustion process images of (a) 0.464, (b) 0.467, and (c) 0.470 g mixture.

retardants is shown in Figure 9a. The SET of the mixture is 111 s g^{-1} when flame retardants are not included. The SET drops to 100, 89, and 90 s g^{-1}, respectively, when 5 wt % APP, ATH−APP, and en-ATH−APP are added to the cathode material. The SET decreases again to 95, 78, and 89 s g^{-1}, respectively, when the flame-retardant content increases to 10 wt %.

Self-extinguishing efficiency (η) was calculated by eq 1:

$$\eta = (t_0 - t)/t_0 \times 100\% \quad (1)$$

where t_0 and t are the SET obtained by burning the mixture in the absence and presence of flame retardants, respectively.[19] The value of η is shown in Figure 9b when various flame retardants are included. It can be seen that the η of en-ATH−APP is higher than that of APP. The η of en-ATH−APP is comparable to that of ATH−APP, which demonstrates that PUF has almost no effect on flame-retardant efficiency. The fire extinguishing test result is consistent with the result of DSC, which manifests that en-ATH−APP has better flame-retardant property because of the synergistic effect of APP and ATH.

2.4. Electrochemical Property of Batteries. To investigate the influence of flame retardants on the electrochemical property of batteries, the battery impedance and capacity were tested. The impedance curves of lithium-ion batteries with 5 and 10 wt % flame retardants are shown in Figure 10. The equivalent circuit is shown in the inset of Figure 10, and the impedance obtained by fitting the equivalent circuit is shown in Table 1. The Nyquist plots contains a semicircle at a high frequency and an oblique line at a low frequency, which are attributed to electrolyte impedance (R_e) and charge-transfer impedance (R_{ct}), respectively.[28] The R_{ct} value of the cathode without flame retardants is 118.3 Ω. The value of R_{ct} is 125.7, 141.7, and 123.4 Ω, respectively, when 5 wt % APP, ATH−APP, and en-ATH−APP are added to the cathode. The R_{ct} has a similar change tendency when the

https://doi.org/10.1021/acsomega.1c00598
ACS Omega 2021, 6, 21227−21234

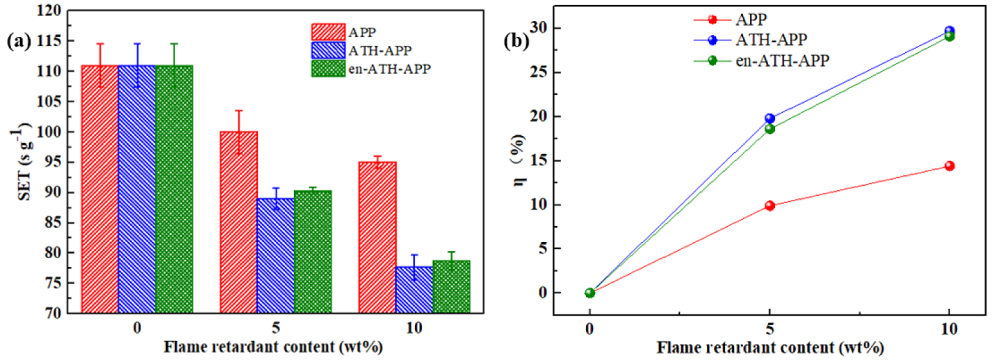

Figure 9. (a) SET and (b) η of the $LiFePO_4$−electrolyte mixture with various flame retardants.

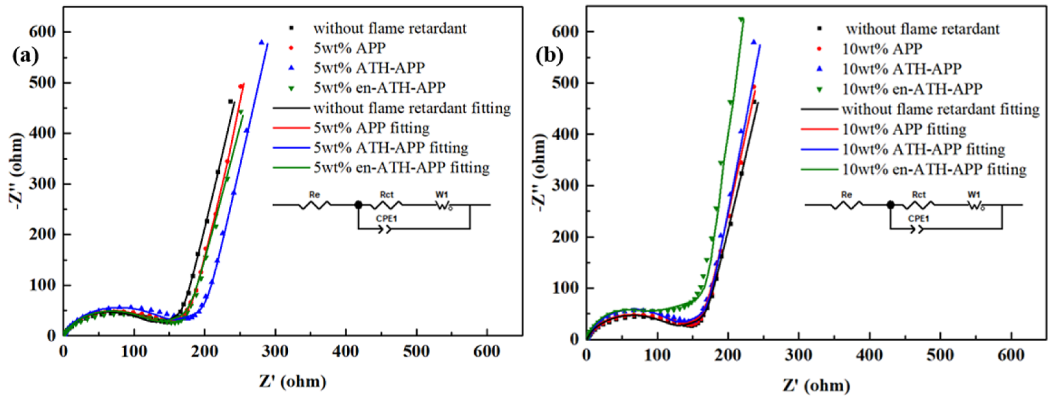

Figure 10. Impedance curves of lithium-ion batteries with (a) 5 wt % flame retardants and (b) 10 wt % flame retardants.

Table 1. Impedance of Lithium-Ion Batteries

	impedance/Ω	
flame retardant content in the cathode	R_e	R_{ct}
without flame retardants	0.75	118.3
5 wt % APP	0.79	125.7
10 wt % APP	0.7	127.6
5 wt % ATH−APP	0.85	141.7
10 wt % ATH−APP	0.93	147.8
5 wt % en-ATH−APP	0.84	123.4
10 wt % en-ATH−APP	1.2	126.2

flame-retardant content increases to 10 wt %, which are 127.6, 147.8, and 126.2 Ω, respectively. The value of R_{ct} is the smallest when en-ATH−APP is added to the cathode. This is because the PUF can inhibit the possible reaction between flame retardants and cathode material. In addition, flame retardants coated with PUF has better dispersion in the cathode material, which promotes the contact between the $LiFePO_4$ and the conductive agent, thereby reducing the impedance.[19]

The charge and discharge curves of batteries with 5 and 10 wt % flame retardants are shown in Figure 11. The battery without flame retardants manifests a stable plateau voltage at 3.4 V and a high specific capacity of 151.71 mAh g^{-1}. The battery has the lowest plateau voltage and capacity, when ATH−APP is added in the cathode. When ATH−APP is coated with PUF, the plateau voltage and capacity of batteries

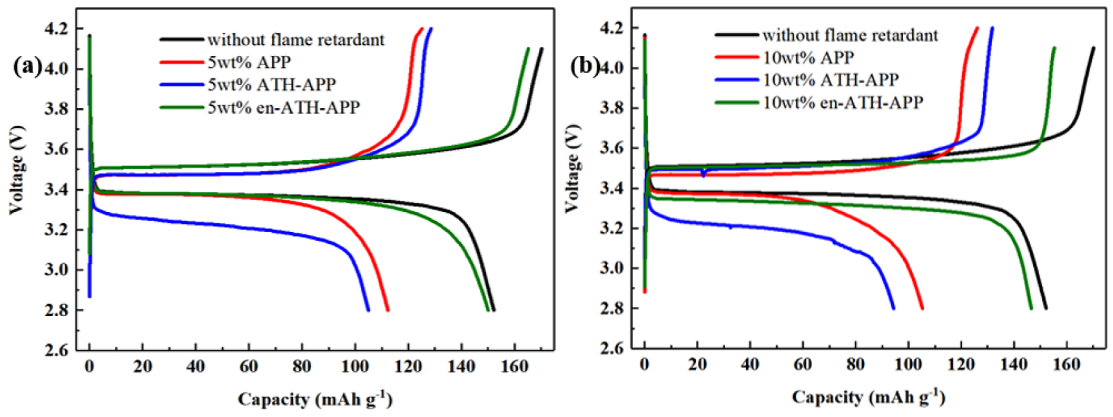

Figure 11. Charge and discharge curves for lithium-ion batteries with (a) 5 and (b) 10 wt % flame retardants.

https://doi.org/10.1021/acsomega.1c00598
ACS Omega 2021, 6, 21227−21234

are improved, which is comparable to the voltage and capacity of the battery without flame retardants. The cycle performance of batteries with and without en-ATH−APP is shown in Figure 12. It can be seen that the battery without the flame retardant

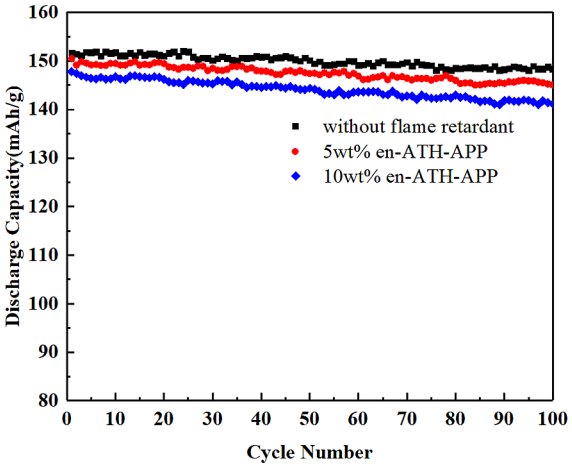

Figure 12. Cycle performance of batteries with and without en-ATH−APP.

has a high capacity retention. The battery discharge capacity is 148.36 mAh g^{-1}, and the battery capacity retention is 97.8% after 100 cycles. With the addition of en-ATH−APP, the discharge capacity of the battery decreased slightly. The discharge capacities of the battery with 5 wt % en-ATH−APP and 10 wt % en-ATH−APP are 145.06 and 141.12 mAh g^{-1}, respectively, after 100 cycles, and the capacity retention rates are 96.4% and 95.5%, respectively. The result of the discharge capacity is consistent with the impedance result. Lithium-ion batteries with APP or ATH−APP have a larger impedance, which results in a decrease in the capacity of the battery. When ATH−APP is covered by PUF, the battery capacity increases because of the decrease in battery impedance.

3. CONCLUSIONS

A synergistic flame-retardant microcapsule based on APP and ATH was prepared by the precipitation method and in situ polymerization and characterized by FTIR spectroscopy and SEM images. Microcapsule flame retardants were added to the electrode, and their influence on the safety of the electrode and the electrochemical property for the lithium-ion batteries was discussed. The results of the thermal stability and flame-retardant property of the electrode demonstrated that en-ATH−APP was better than APP in improving electrode safety because of the synergistic effect of APP and ATH. Moreover, the flame-retardant efficiency of en-ATH−APP was comparable to that of ATH−APP, which indicates that PUF had almost no effect on flame-retardant property. In terms of electrochemical property, the cathode with en-ATH−APP showed lower impedance than that with APP and ATH−APP. The reason for this phenomenon may be that the presence of PUF improves the dispersion of flame retardants in the cathode and thus reduces the impedance. Because of the reduction of the transfer impedance, the lithium-ion battery with en-ATH−APP has a higher discharge capacity than that with APP and ATH−APP, and the battery capacity retention is 96.4% and 95.5%, respectively, after 100 cycles when the contents of en-ATH−APP are 5 wt % and 10 wt%. This article provides a new idea for the application of flame retardants in lithium-ion batteries.

4. EXPERIMENTAL SECTION

4.1. Synthesis of Microcapsule Flame Retardants. The synthesis of en-ATH−APP involves two steps. First, the ATH shell was formed on the surface of APP (Aladdin, 99%) by the precipitation method. The reagents such as APP (12 g) and polyethylene glycol *tert*-octylphenyl ether (0.1 g) (OP-10; Macklin, 99%) were dissolved in 70 mL of ethanol (Aladdin, 98%). In the meantime, 4 g of aluminum chloride (Aladdin, 99%) was dissolved in 20 mL of deionized water to prepare a solution of aluminum chloride. The aluminum chloride solution was added to the previous ethanol solution under stirring. The pH of previous ethanol solution was adjusted to 7.5 by 10 wt % sodium bicarbonate (Sinopharm, 99.5%) solution. Then, the mixed solution was reacted for 2 h under stirring. The surface of APP was coated with a layer of ATH because of Al^{3+} precipitation under weak alkaline conditions. The formed intermediate product ATH−APP was filtered, washed, and dried.[23]

Second, a layer of the PUF shell was coated on the surface of ATH−APP through in situ polymerization. Formaldehyde (6 g) solution (Xilong, 37%) was mixed with 2 g of urea (Macklin, 99%) and stirred until the urea dissolved. The pH of the solution was adjusted to 8.5 with 10 wt % sodium bicarbonate solution. Then, the solution was reacted for 1.5 h at 70 °C to obtain the urea-formaldehyde prepolymer. ATH−APP (8 g) and 0.5 g of OP-10 were added to 65 mL of ethanol, and the ethanol solution was stirred for 40 min. Urea-formaldehyde prepolymer solution, 0.3 g of resorcinol (Sinopharm, 98%), and 0.3 g of ammonia chloride (Xilong, 99.5%) were added into the ethanol solution. The pH of the solution was adjusted to 3 by acetic acid (Shenbo, 99.5%), and then, the solution was stirred for 3 h at 60 °C. Microcapsule flame retardants were separated from the solution and washed repeatedly with deionized water.[29]

4.2. Characterization of Microcapsule Flame Retardants. The surface chemistries of the microcapsules were characterized by FTIR (Nicolet iS20). The KBr tablet with microcapsules was tested by the transmission method in the scanning range of 400−4000 cm^{-1}. The microstructure of the microcapsule was examined through an SEM (Hitachi S-4700).

4.3. Thermal Stability and Flame-Retardant Property of the Electrode. The thermal stability of the electrode was tested by DSC. The $LiFePO_4$ with 0% SOC and the electrolyte were mixed in a mass ratio of 3:1, and then, the mixture was characterized by HP-DSC1 (Mettler Toledo) at a heating rate of 10 °C min^{-1}. The effect of microcapsule flame retardants on the thermal stability of $LiFePO_4$ with 100% SOC was also studied because the thermal stability of electrode materials decreased with an increase in SOC.[30,31] The battery with $LiFePO_4$ as the cathode was disassembled when $LiFePO_4$ was charged to 100% SOC. Then, the $LiFePO_4$ was scraped from the current collector, and the mixture of the $LiFePO_4$ with 100% SOC and the electrolyte in a ratio of 3:1 was characterized by HP-DSC1 at a heating rate of 10 °C min^{-1}. The effect of microcapsule flame retardants on the thermal stability of graphite anodes with 100% SOC was further studied in this article. The battery with graphite as the anodes was disassembled when graphite was charged to 100% SOC. Then, the graphite was scraped from the current collector and characterized by HP-DSC1 at a heating rate of 10 °C min^{-1}.

https://doi.org/10.1021/acsomega.1c00598
ACS Omega 2021, 6, 21227−21234

Flame-retardant property was tested by fire extinguishing test of the $LiFePO_4$−electrolyte mixture. The $LiFePO_4$ with 0% SOC and the electrolyte were mixed in a mass ratio of 3:1, then the mixture was placed in a glass dish (diameter = 12 cm), and ignited in the atmosphere to record the SET.

4.4. Electrochemical Measurement of Batteries with Microcapsule Flame Retardants. APP encapsulated by ATH and PUF in sequence was used as flame-retardant additives for the cathode. The oil-based cathode slurry with $LiFePO_4$ powders was prepared by mixing with carbon black (Super-P; Timcal), polyvinylidene difluoride (PVDF; Sigma-Aldrich), and flame retardants. $LiFePO_4$, Super-P, and flame retardants were mixed and ground for 1 h in a ball crusher (QM-3SP4, Laibu, China). The PVDF was dissolved in the *N*-methyl pyrrolidone solution (Macklin, 99%), and then, the $LiFePO_4$ mixture was added to the solution. The cathode slurry was stirred for 1 h at room temperature. After the cathode slurry was fully mixed, the slurry was coated on an aluminum foil through a blade coater. The coated aluminum foil was dried in a vacuum drying oven for 12 h at 80 °C. The dried aluminum foil was cut into a positive sheet through a bead machine. In the dried electrode sheet, the mass ratio of $LiFePO_4$, Super-P, and PVDF was 8:1:1. Flame retardants occupied 5 and 10 wt % of the total mass of the positive electrode material.

The effect of flame retardants on the battery property was tested in CR2032 coin cells. The cathode was the $LiFePO_4$ electrode sheet, lithium foil was used as the anode, and polypropylene (Celgard 2500) was chosen as the separator. A solution of 1 M $LiPF_6$ in a mixture of 1:1:1 (v/v) ethylene carbonate, ethyl methyl carbonate, and dimethyl carbonate was selected as the electrolyte. The CR2032 lithium coin cell was assembled in a glovebox filled with argon.

The assembled battery was placed for 10 h, so that the open-circuit voltage of the battery reached a stable state. Then, the discharge capacity and electrochemical impedance spectroscopy (EIS) of the battery were tested. The discharge capacity of the coin cells was evaluated by the battery testing system (CT-4000, Neware, China). The battery was measured by charging the battery to 4.2 V and then discharging to 2.5 V at a constant current of 0.5 C. The EIS was tested through the electrochemical workstation (CHI 627D, Chenhua, China). The scanning frequency was in the range of 10^5−0.01 Hz, and the perturbation amplitude was 10 mV.

AUTHOR INFORMATION

Corresponding Author

Jia-Jia Jiang − *Jiangsu Key Laboratory of Hazardous Chemicals Safety and Control, College of Safety Science and Engineering, Nanjing Tech University, Nanjing 211816, China;* orcid.org/0000-0002-6796-6913; Email: jiajiajiang@njtech.edu.cn

Authors

Teng-Kun Ma − *Jiangsu Key Laboratory of Hazardous Chemicals Safety and Control, College of Safety Science and Engineering, Nanjing Tech University, Nanjing 211816, China*

Yu-Man Yang − *College of Materials and Engineering, Nanjing Tech University, Nanjing 211816, China*

Meng Yang − *College of Materials and Engineering, Nanjing Tech University, Nanjing 211816, China*

Jun-Cheng Jiang − *Jiangsu Key Laboratory of Hazardous Chemicals Safety and Control, College of Safety Science and Engineering, Nanjing Tech University, Nanjing 211816, China*

Complete contact information is available at: https://pubs.acs.org/10.1021/acsomega.1c00598

Notes

The authors declare no competing financial interest.

ACKNOWLEDGMENTS

This work was supported by the National Natural Science Foundation of China (no. 51804167), the Natural Science Foundation of Jiangsu (no. BK20150953), and the Practice Innovation Program of Jiangsu Province (SJCX20_0374).

REFERENCES

(1) Xiong, R.; Ma, S. X.; Li, H. L.; Sun, F. C.; Li, J. Toward a safer battery management system: A critical review on diagnosis and prognosis of battery short circuit. *iScience* **2020**, *23*, 1−18.

(2) Xiong, R.; Sun, W. Z.; Yu, Q. Q.; Sun, F. C. Research progress, challenges and prospects of fault diagnosis on battery system of electric vehicles. *Appl. Energy* **2020**, *279*, No. 115855.

(3) Wang, Y. W.; Peng, P.; Cao, W. J.; Dong, T.; Zheng, Y. D.; Lei, B.; Shi, Y. J.; Jiang, F. M. Experimental study on a novel compact cooling system for cylindrical lithium-ion battery module. *Appl. Therm. Eng.* **2020**, *180*, 1−10.

(4) Abada, S.; Marlair, G.; Lecocq, A.; Petit, M.; Sauvant-Moynot, V.; Huet, F. Safety focused modeling of lithium-ion batteries: A review. *J. Power Sources* **2016**, *306*, 178−192.

(5) Zeyu, C.; Xiong, R.; Fengchun, S. Research status and analysis for battery safety accidents in electric vehicles. *Chin. J. Mech. Eng. (Engl. Ed.)* **2019**, *55*, 93−104.

(6) Shiga, T.; Kato, Y.; Kondo, H.; Okuda, C. A. Self-extinguishing electrolytes using fluorinated alkyl phosphates for lithium batteries. *J. Mater. Chem. A* **2017**, *5*, 5156−5162.

(7) Ferry, A.; Edman, L.; Forsyth, M.; MacFarlane, D. R.; Sun, J. Z. NMR and Raman studies of a novel fast-ion-conducting polymer-in-salt electrolyte based on $LiCF_3SO_3$ and PAN. *Electrochim. Acta* **2000**, *45*, 1237−1242.

(8) Jimenez, R.; Rivera, A.; Várez, A.; Sanz, J. Li mobility in $Li_{0.5-x}Na_xLa_{0.5}TiO_3$ perovskites ($0 \le x \le 0.5$): Influence of structural and compositional parameters. *Solid State Ionics* **2009**, *180*, 1362−1371.

(9) Zhong, G. B.; Wang, Y.; Wang, C.; Wang, Z. H.; Guo, S.; Wang, L. J.; Liang, X.; Xiang, H. F. An AlOOH-coated polyimide electrospun fibrous membrane as a high-safety lithium-ion battery separator. *Ionics* **2019**, *25*, 2677−2684.

(10) Shi, C.; Dai, J. H.; Li, C.; Shen, X.; Peng, L. Q.; Zhang, P.; Wu, D. Z.; Sun, D. H.; Zhao, J. B. A modified ceramic-coating separator with high-temperature stability for lithium-ion battery. *Polymers* **2017**, *9*, 1−12.

(11) Lia, Y.; Liu, X.; Ren, D. S.; Hsu, H. J.; Xu, G. L.; Hou, J. X.; Wang, L.; Feng, X. N.; Lu, L. G.; Xu, W. Q.; Ren, Y.; Li, R. H.; He, X. M.; Amine, K.; Ouyang, M. G. Toward a high-voltage fast-charging pouch cell with TiO2 cathode coating and enhanced battery safety. *Nano Energy* **2020**, *71*, No. 104643.

(12) Rejina Parvin, J.; Gokul Kumar, S.; Elakya, A.; Priyadharsini, K.; Sowmya, R. Nickel material based battery life and vehicle safety management system for automobiles. *Mater. Today: Proc.* **2020**, *37*, 2844−2847.

(13) Yao, X. L.; Xie, S.; Chen, C. H.; Wang, Q. S.; Sun, J. H.; Li, Y. L.; Lu, S. X. Comparative study of trimethyl phosphite and trimethyl phosphate as electrolyte additives in lithium ion batteries. *J. Power Sources* **2005**, *144*, 170−175.

(14) Xu, K.; Ding, M. S.; Zhang, S. S.; Allen, J. L.; Jow, T. R. An attempt to formulate nonflammable lithium ion electrolytes with alkyl

phosphates and phosphazenes. *J. Electrochem. Soc.* **2002**, *149*, A622−A626.
(15) Wang, W.; Liao, C.; Liu, L. X.; Cai, W.; Yuan, Y.; Hou, Y. B.; Guo, W. W.; Zhou, X.; Qiu, S. L.; Song, L.; Kan, Y. C.; Hu, Y. Comparable investigation of tervalent and pentavalent phosphorus based flame retardants on improving the safety and capacity of lithium-ion batteries. *J. Power Sources* **2019**, *420*, 143−151.
(16) Hogstroem, K. C.; Lundgren, H.; Wilken, S.; Zavalis, T. G.; Behm, M.; Edstrom, K.; Jacobsson, P.; Johansson, P.; Lindbergh, G. Impact of the flame retardant additive triphenyl phosphate (TPP) on the performance of graphite/$LiFePO_4$ cells in high power applications. *J. Power Sources* **2014**, *256*, 430−439.
(17) Chen, C. A.; Li, C. C. Microencapsulating inorganic and organic flame retardants for the safety improvement of lithium-ion batteries. *Solid State Ionics* **2018**, *323*, 56−63.
(18) Huang, P. H.; Chang, S. J.; Li, C. C. Encapsulation of flame retardants for application in lithium-ion batteries. *J. Power Sources* **2017**, *338*, 82−90.
(19) Baginska, M.; Sottos, N. R.; White, S. R. Core−shell microcapsules containing flame retardant tris(2-chloroethyl phosphate) for lithium-ion battery applications. *ACS Omega* **2018**, *3*, 1609−1613.
(20) Chen, M.; Tang, M. Q.; Qi, F.; Chen, X. L.; He, W. D. Microencapsulated ammonium polyphosphate and its application in the flame retardant polypropylene composites. *J. Fire Sci.* **2015**, *33*, 374−389.
(21) Zhao, R. J.; Liu, Y. J.; Zhang, L. Structure and properties of halogen-free flame retardant ethylene-vinyl acetate copolymer with aluminum hydroxide. *China Plastics* **2018**, *32*, 97−102.
(22) Liang, S. J.; Xu, H. S. Halogen-free flame retardant polypropylene composites. *Plastics* **2009**, *38*, 19−21.
(23) Zhao-Lu, Q.; Ding-Hua, D. H.; Rong-Jie, Y. Preparation of ammonium polyphosphate coated with aluminium hydroxide and its application in polypropylene as flame retardant. *J. Inorg. Mater.* **2015**, *30*, 1267−1272.
(24) Priya, G. K.; Padmaja, P.; Warrier, K. G. K.; Damodaran, A. D.; Aruldhas, G. Dehydroxylation and high temperature phase formation in sol-gel boehmite characterized by fourier transform infrared spectroscopy. *J. Mater. Sci. Lett.* **1997**, *16*, 1584−1587.
(25) Li, D. Y.; Yang, H.; Xie, T. T.; Guo, X. Z.; Lian, J. S. The heat treatment process of hydrous alumina and characteristics of nanometer Al_2O_3. *Chin. J. Inorg. Chem.* **2006**, *22*, 96−100.
(26) Yuan, L.; Liang, G. Z.; Xie, J. Q.; Li, L.; Guo, J. Preparation and characterization of poly(urea-formaldehyde) microcapsules filled with epoxy resins. *Polymer* **2006**, *47*, 5338−5349.
(27) Castrovinci, A.; Camino, G.; Drevelle, C.; Duquesne, S.; Magniez, C.; Vouters, M. Ammonium polyphosphate−aluminum trihydroxide antagonism in fire retarded butadiene−styrene block copolymer. *Eur. Polym. J.* **2005**, *41*, 2023−2033.
(28) Zhao, X. M.; Yan, Y. W.; Ren, X. X.; Chen, L.; Xu, S. D.; Liu, S. B.; Wang, X. M.; Zhang, D. Trimethyl phosphate for nonflammable carbonate-based electrolytes for safer room-temperature sodium-sulfur batteries. *ChemElectroChem* **2019**, *6*, 1229−1234.
(29) Lai, G. W.; Chang, S. J.; Lee, J. T.; Liu, H.; Li, C. C. Conductive microcapsules for self-healing electric circuits. *RSC Adv.* **2015**, *5*, 104145−104148.
(30) Cai, W.; Wang, H.; Maleki, H.; Howard, J.; Lara-Curzio, E. Experimental simulation of internal short circuit in Li-ion and Li-ion-polymer cells. *J. Power Sources* **2011**, *196*, 7779−7783.
(31) Qingsong, Z.; Chaochao, G.; Shuaixing, Q. Study on lithium-ion batteries explosive characteristics and aviation transportation safety. *China Saf. Sci. J.* **2016**, *26*, 50−55.

https://doi.org/10.1021/acsomega.1c00598
ACS Omega 2021, 6, 21227−21234